

Image Deraining with Frequency-Enhanced State Space Model

Shugo Yamashita and Masaaki Ikehara

Keio University, Yokohama, Japan

Abstract. Removing rain artifacts in images is recognized as a significant issue. In this field, deep learning-based approaches, such as convolutional neural networks (CNNs) and Transformers, have succeeded. Recently, State Space Models (SSMs) have exhibited superior performance across various tasks in both natural language processing and image processing due to their ability to model long-range dependencies. This study introduces SSM to rain removal and proposes a Deraining Frequency-Enhanced State Space Model (DFSSM). To effectively remove rain streaks, which produce high-intensity frequency components in specific directions, we employ frequency domain processing concurrently with SSM. Additionally, we develop a novel mixed-scale gated-convolutional block, which uses convolutions with multiple kernel sizes to capture various scale degradations effectively and integrates a gating mechanism to manage the flow of information. Finally, experiments on synthetic and real-world rainy image datasets show that our method surpasses state-of-the-art methods.

1 Introduction

Images captured under rainy conditions suffer from deteriorated visual quality. Rain-related degradations adversely affect the performance of downstream tasks such as object detection, object tracking, and segmentation, as well as the overall effectiveness of vision applications that employ these algorithms. Removing rain artifacts in images enhances both the performance and reliability of vision systems.

Single image deraining has been extensively studied for its usefulness. Recently, deep learning-based approaches have significantly advanced its performance. Convolutional neural network (CNN)-based methods [1,2,3,4,5,6,7,8,9,10] surpassed the previous handcrafted prior methods. However, CNNs cannot capture global features because they collect features from local regions using fixed-size kernels. Subsequently developed, Transformer [11] employs the attention mechanism that captures global information and enables inference based on input features. In the deraining task, Transformer-based methods [12,13,14,15] demonstrated promising performance. Nonetheless, the attention mechanism demands quadratic complexity relative to input image sizes. To mitigate computational complexity, self-attention is calculated across channels instead of spatial dimension [12], within localized window regions [13], or sparsely [14,15].

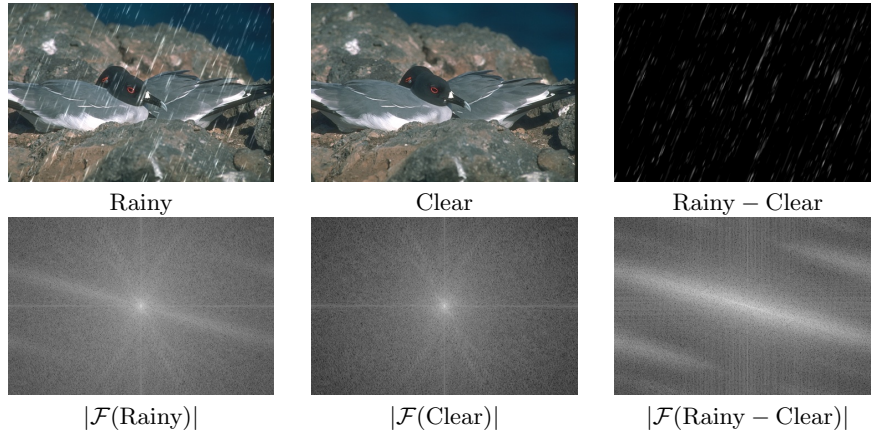


Fig. 1. Top row: a rainy image, a clear image, and their differential image. Bottom row: Corresponding 2D Fourier amplitude spectra. The amplitude of the Fourier transform is denoted as $|\mathcal{F}(\cdot)|$.

Recently, State Space Models (SSMs) [16,17] have emerged as innovative architectures for deep neural networks. SSMs conduct sequence-to-sequence transformation using hidden states to interact with previously scanned elements, thereby modeling long-range dependencies with linear complexity. Mamba [17] enhances this architecture by treating parameters of SSMs as functions of the input, realizing content-driven inference. Mamba [17] architecture, initially designed for one-dimensional data in natural language processing, is applied for image processing by flattening two-dimensional images into one-dimensional sequences. Its effectiveness has been demonstrated in image recognition [18,19,20,21], image restoration [22,23], and medical image segmentation [24,25].

In this paper, we propose a novel Deraining Frequency-Enhanced State Space Model (DFSSM). We use the SSM as the primary architecture, which provides a global receptive field and content-based reasoning with linear computation. We also employ frequency domain processing. Separate processing of high-frequency components, which represent edges, details, and textures, and low-frequency components, which represent smooth and gradual variations helps to restore images. As depicted in Fig. 1, 2D Fourier amplitude spectra of a pair of rainy and clear images reveals strong features in the direction orthogonal to rain streaks. Thus, frequency domain processing works effectively to remove rain streaks. Specifically, we proposed a Frequency-Enhanced State Space Block (FSSB), which uses a Fast Fourier Transform Module (FFTM) for frequency domain processing in parallel with a Vision State Space Module (VSSM) for SSM operations. During training, a Frequency Reconstruction loss [26,27] is adopted to promote learning based on frequency components. Furthermore, a Mixed-Scale Gated-Convolutional Block (MGCB) is used to capture local features. Convolutions with multiple kernel sizes are employed to process diverse scales of rain

streaks effectively. Concurrently, adopting a gating mechanism enables the selective transmission of features.

Comprehensive experiments are conducted to evaluate the proposed DFSSM. On the heavy rain streak dataset Rain200H [28] and the light rain streak dataset Rain200L [28] and the real-world rainy image dataset SPA-Data [29], our method achieves quantitatively and qualitatively superior performance compared to state-of-the-art methods. Ablation studies demonstrate that the proposed improvements are effective for removing rain artifacts.

The contributions of this paper are summarized as follows:

- We propose a Deraining Frequency-Enhanced State Space Model (DFSSM). Our method uses a Frequency-Enhanced State Space Block (FSSB) containing a Vision State Space Module (VSSM) and a Fast Fourier Transform Module (FFTM) for effective rain degradation removal.
- We develop a Mixed-Scale Gated-Convolutional Block (MGCB), which effectively captures various scale degradations through mixed-scale convolutions and manages the flow of features using a gating mechanism.
- Experimental results show that our method achieves state-of-the-art performance on synthetic and real-world rainy image datasets.

2 Related Works

2.1 Image Deraining

Extensive research has been conducted to restore rain-degraded images. Traditional methods [30,31,32,33,34] separate a rainy image into the background and rain layers with various handcrafted priors, such as discriminative sparse coding [31] and Gaussian mixture model [32]. However, these prior-based approaches have difficulty dealing with complex rain forms.

Currently, deep learning-based methods are the dominant approaches for removing rain streaks. Initially, CNN-based methods [1,2,3,4,5,6,7,8,9,10] were extensively studied. DDN [1] used a deep convolutional neural network, focusing on high-frequency detail during training. Recursive computation [2,3,4,5] and multi-scale representation [4,5,6] were successfully deployed to remove rain streaks. RCDNet [7] proposed interpretable network architecture with a convolutional dictionary learning model. CCN [8] explored a network that removes both rain streaks and raindrops with a neural architecture search [35]. DualGCN [9] used dual graph convolutional networks to consider long-range contextual information. SPDNet [10] employed a wavelet-based feature extraction backbone with a residue channel prior guided mechanism.

Recent studies [12,13,14,15] have applied Transformer [11] to deraining. These methods are designed to reduce the computational quadratic complexity of vanilla self-attention. Restormer [12] applied self-attention across channels rather than the spatial dimension. IDT [13] used a window-based Transformer and a spatial Transformer to extract local and global features. A sparse attention mechanism, which calculates attention using only highly relevant elements rather than

all elements, is introduced to rain removal along with a learnable top-k selection operator [14] and an uncertainty-driven ranking strategy [15].

2.2 State Space Models

State Space Models (SSMs), recently incorporated into deep learning from classical control theory, are designed for sequence-to-sequence transformation. Structured State Spaces model (S4) [16] handles long sequences effectively with linear computation. Mamba [17] enabled content-driven inference with parameters of SSMs as functions of the input and achieved state-of-the-art performance in the natural language domain. Vim [18] and VMamba [19], which adapted Mamba to the field of image recognition, transform 2D images into 1D sequences by scanning with multiple routes and then using SSMs. LocalMamba [20] improves the scan direction and enhances the ability to capture local 2D relationships. EfficientVMamba [21] proposed a lightweight model. SSMs have also been applied in medical image segmentation [24,25] and image restoration [22,23]. In this study, we utilize SSM with frequency enhancement to restore images degraded by rain.

3 Preliminaries

In continuous linear time-invariant systems (LTI), SSMs project a 1D input sequence $x(t) \in \mathbb{R}^L$ into a 1D output sequence $y(t) \in \mathbb{R}^L$ via a latent state $h(t) \in \mathbb{R}^N$. These models are formulated as linear ordinary differential equations:

$$h'(t) = Ah(t) + Bx(t), \quad (1)$$

$$y(t) = Ch(t) + Dx(t), \quad (2)$$

where the parameters include $A \in \mathbb{R}^{N \times N}$, $B \in \mathbb{R}^{N \times 1}$, $C \in \mathbb{R}^{1 \times N}$, and the skip connection $D \in \mathbb{R}^1$.

To incorporate SSMs into deep learning algorithms, the continuous differential equations are discretized. Define $\Delta \in \mathbb{R}$ as a timescale parameter, the continuous parameters A and B are transformed into discrete parameters \bar{A} and \bar{B} using the zeroth-order hold rule:

$$\bar{A} = \exp(\Delta A), \quad (3)$$

$$\bar{B} = (\exp^{\Delta A} - I)A^{-1}B \approx (\Delta A)(\Delta A)^{-1}\Delta B = \Delta B, \quad (4)$$

$$h_k = \bar{A}h_{k-1} + \bar{B}x_k, \quad (5)$$

$$y_k = Ch_k + Dx_k, \quad (6)$$

where \bar{B} is approximated by the first-order Taylor series.

Mamba [17] introduces a selective State Space Model (S6), which enable a dynamic feature representation by parameterizing B , C , and Δ as functions of the input. In addition, parallel scanning facilitates efficient parallel processing. Designed for image processing, a 2D Selective Scan Module (2D-SSM) [19,22]

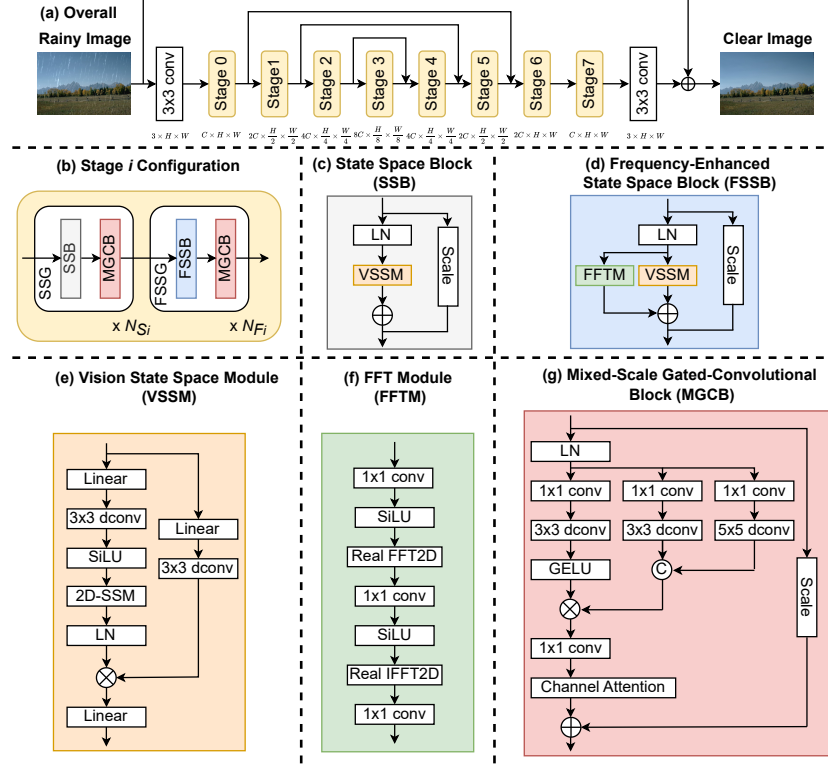


Fig. 2. The architecture of our Deraining Frequency-Enhanced State Space Model (DFSSM). The overall U-Net architecture (a) has 8 stages. The i th stage (b) consists of N_{S_i} State Space Groups (SSGs) and N_{F_i} Frequency-Enhanced State Space Groups (FSSGs). (c), (d), (e), (f), and (g) illustrate the details of the components. The SSG includes a State Space Block (SSB) and a Mixed-Scale Gated-Convolutional Block (MGCb), while the FSSG includes a Frequency-Enhanced State Space Block (FSSB) and an MGCb. Both SSB and FSSB employ a Vision State Space Module (VSSM), and the FSSB also uses a Fast Fourier Transform Module (FFTM).

flattens 2D images into four 1D sequences by scanning along four distinct directions: top-left to bottom-right, bottom-right to top-left, top-right to bottom-left, and bottom-left to top-right. These sequences are applied to the SSMs individually and then merged.

4 Proposed Method

4.1 Overall Pipeline

The overall architecture of the proposed Deraining Frequency-Enhanced State Space Model (DFSSM) is illustrated in Fig. 2. Given a rainy input image $I \in \mathbb{R}^{3 \times H \times W}$, our deraining network removes degradations and outputs a clear image $\hat{I} \in \mathbb{R}^{3 \times H \times W}$. Our hierarchical encoder-decoder network employs SSMs with MambaIR [22] as the baseline.

We employ a U-Net [36] architecture akin to Restormer [12], comprising 8 stages across four resolution levels: $H \times W$, $\frac{H}{2} \times \frac{W}{2}$, $\frac{H}{4} \times \frac{W}{4}$ and $\frac{H}{8} \times \frac{W}{8}$. Initially, the input image I undergoes channel expansion from 3 to C via a 3×3 convolution. Then, the encoder and decoder are applied, processing features while decreasing and increasing resolution, respectively. Downsampling and up-sampling of image sizes are conducted through pixel-unshuffle and pixel-shuffle techniques [37]. Skip connections facilitate the integration of features from the encoder into the decoder. After the skip connections at $\frac{H}{2} \times \frac{W}{2}$ and $\frac{H}{4} \times \frac{W}{4}$ resolution levels, the channels are halved through a 1×1 convolution. The features from the decoder are fed into a refinement stage operating at high resolution. Finally, applying a 3×3 convolution and adding skip connection from the input image I , we obtain the clear image \hat{I} .

Each encoder, decoder, and refinement stage comprises N_{S_i} State Space Groups (SSGs) and N_{F_i} Frequency-Enhanced State Space Groups (FSSGs), where i -th is the order in the model. The SSG is a series connection of a State Space Block (SSB) and a Mixed-Scale Gated-Convolutional Block (MGCB). The FSSG is a series connection of a Frequency-Enhanced State Space Block (FSSB) and an MGCB. The following describes the components and loss functions of our model in detail.

4.2 State Space Block (SSB)

We employ the State Space Model (SSM) to remove rain artifacts. The SSM can capture global information with linear complexity. Following MambaIR [22], the State Space Block (SSB), shown in Fig. 2(c), contains a layer normalization, a Vision State Space Module (VSSM), and a skip connection using a learnable scale factor. Given the input tensor X , the SSB can be defined as:

$$X_{out} = \text{VSSM}(\text{LN}(X)) + s \cdot X, \quad (7)$$

where LN represents the layer normalization and s denotes the learnable scale factor. In the VSSM [19] (Fig. 2(e)), a 2D Selective Scan Module scans 2D feature maps in four distinct directions, flattening them into 1D sequences. Then, each sequence is processed by SSM, and the outcomes are merged.

4.3 Frequency-Enhanced State Space Block (FSSB)

Transforming an image into the frequency domain allows separation of high-frequency signals, representing fine details and textures, and low-frequency signals, corresponding to flat regions. Separately processing these distinct features

within the frequency domain enhances the model expressiveness, as successfully demonstrated by [27,38,39]. Fig. 1 shows 2D Fourier amplitude spectra of a rain image, a clear image, and their difference image. Components in the direction orthogonal to rain streaks exhibit higher values. Consequently, it can be expected that frequency domain processing helps to remove rain streaks. Motivated by these insights, we introduce the Frequency-Enhanced State Space Block (FSSB), which expands the SSB. As shown in Fig. 2(d), the FSSB uses a Fast Fourier Transform Module (FFTM) in parallel with the VSSM:

$$X_{out} = \text{VSSM}(\text{LN}(X)) + \text{FFTM}(\text{LN}(X)) + s \cdot X. \quad (8)$$

In the FFTM (Fig. 2(f)), we initially use a 1×1 convolution that halves the channel and a SiLU activation function [40] to obtain the suitable feature map for processing in the frequency domain. Subsequently, a Fast Fourier Transform (FFT) transforms the feature map from the spatial domain to the frequency domain. Given that the image features are represented as a real tensor, a 2D Real FFT is used to reduce computational complexity by exploiting symmetry. To extract features in the frequency domain, we use a 1×1 convolution with a SiLU. Then, a 2D Real Inverted FFT (IFFT) is used to bring it back from the frequency domain to the spatial domain. Finally, a 1×1 convolution expands the channels to the original number of channels. Given the input features Z , the FFTM process is defined as:

$$\hat{Z} = \text{SiLU}(1 \times 1 \text{ Conv}(Z)), \quad (9)$$

$$Z_f = \mathcal{F}^{-1}(\text{SiLU}(1 \times 1 \text{ Conv}(\mathcal{F}(\hat{Z})))), \quad (10)$$

$$Z_{out} = 1 \times 1 \text{ Conv}(Z_f), \quad (11)$$

where \mathcal{F} and \mathcal{F}^{-1} denote the 2D Real FFT and IFFT.

4.4 Mixed-Scale Gated-Convolutional Block (MGCB)

SSB and FSSB can capture the spatial long-term dependency. After these components, we use the Mixed-Scale Gated-Convolutional Block (MGCB) for its proficiency in gathering local details. MGCB contains depth-wise convolutions, aggregating information from spatially neighboring pixels. To remove rain degradations of various scales, multi-scale representation [4,5,6] and convolutions [14] are effective. Hence, we adopt multiple kernel sizes for depthwise-convolution. Following [12], this convolutional block incorporates a gating mechanism. This gating mechanism allows the passage of crucial information while blocking non-essential information, thereby managing the flow of information at each hierarchical level.

Specifically, the MGCB is depicted in Fig. 2(g). The input tensor X is applied a layer normalization and fed into three parallel branches: a gate branch, a 3×3 dconv branch, and a 5×5 dconv branch. Within these branches, the channels are initially expanded by factors of γ , $\frac{\gamma}{2}$, and $\frac{\gamma}{2}$, respectively, through

1×1 convolutions. γ is a hyperparameter of the expansion rate. In the gate branch, a 3×3 depth-wise convolution followed by a GELU activation function [41] is conducted to get X_{gate} . In the 3×3 and 5×5 dconv branches, 3×3 and 5×5 depth-wise convolutions are performed with output $X_{3 \times 3}$ and $X_{5 \times 5}$, respectively. In the process of integrating these branches, $X_{3 \times 3}$ and $X_{5 \times 5}$ are concatenated on a channel-wise basis, subsequently taking the element-wise product with X_{gate} . Then, a 1×1 convolution is conducted to restore the channel dimension. Furthermore, we use a channel attention [42] to consider global context in this block. Last, a skip connection with a learnable scale factor is added to obtain X_{out} . In conclusion, the MGCB can be formulated as:

$$X_{gate} = \text{GELU}(3 \times 3 \text{ DW-Conv}(\text{LN}(X))), \quad (12)$$

$$X_{3 \times 3} = 3 \times 3 \text{ DW-Conv}(\text{LN}(X)), \quad (13)$$

$$X_{5 \times 5} = 5 \times 5 \text{ DW-Conv}(\text{LN}(X)), \quad (14)$$

$$X_{out} = \text{CA}(X_{gate} \odot [X_{3 \times 3}, X_{5 \times 5}]) + s \cdot X, \quad (15)$$

where DW-Conv denotes depth-wise convolution, CA stands for the channel attention, and $[\cdot]$ represents the channel-wise concatenation.

4.5 Loss Functions

The loss function of our method is calculated based on the model output \hat{I} and the ground truth G . We use an L1-loss and a Frequency Reconstruction loss [26,27]. The L1-loss is formulated as:

$$\mathcal{L}_{L1} = \|\hat{I} - G\|_1, \quad (16)$$

where $\|\cdot\|_1$ is the L1 norm. The Frequency Reconstruction loss [26,27] computes the loss at each frequency component:

$$\mathcal{L}_{Freq} = \|\mathcal{F}(\hat{I}) - \mathcal{F}(G)\|_1 \quad (17)$$

where $\mathcal{F}(\cdot)$ denotes the 2D Real Fast Fourier Transform. The total loss is:

$$\mathcal{L}_{total} = \mathcal{L}_{L1} + \lambda_f \mathcal{L}_{Freq}, \quad (18)$$

where λ_f are coefficients to adjust the ratio of the losses.

5 Experiments

5.1 Experimental settings

Datasets We evaluate our deraining method on existing synthetic and real-world datasets. Each dataset contains image pairs; one is degraded by rain, and the other is the same scene without rain. Rain200H and Rain200L [28] include images of synthetic heavy and light rain streaks, respectively. Both datasets have 1,800 training image pairs and 200 test image pairs. SPA-Data [29] is a real-world rainy image dataset and contains 638,492 training image pairs and 1,000 test image pairs.

Table 1. Quantitative results on the Rain200H, Rain200L [28], and SPA-Data [29].

Architecture	Method	Rain200H [28]		Rain200L [28]		SPA-Data [29]	
		PSNR \uparrow	SSIM \uparrow	PSNR \uparrow	SSIM \uparrow	PSNR \uparrow	SSIM \uparrow
Prior	DSC [31]	27.16	0.866	14.73	0.382	34.95	0.942
	GMM [32]	14.50	0.416	28.66	0.865	34.30	0.943
CNN	DDN [1]	26.05	0.806	34.93	0.958	36.16	0.946
	RESCAN [2]	26.75	0.835	36.09	0.970	38.11	0.971
	PreNet [3]	29.04	0.899	37.80	0.981	40.16	0.982
	MSPFN [4]	29.36	0.903	38.58	0.983	43.43	0.984
	RCDNet [7]	30.24	0.905	39.17	<u>0.989</u>	43.36	0.983
	MPRNet [6]	30.67	0.911	39.49	0.983	43.64	0.984
	CCN [8]	29.99	0.914	38.26	0.981	41.94	0.977
	DualGCN [9]	31.15	0.913	40.73	<u>0.989</u>	48.18	0.990
	SPDNet [10]	31.28	0.920	40.50	0.988	43.20	0.987
Transformer	Restormer [12]	31.39	0.916	40.58	0.987	47.98	0.992
	IDT [13]	32.10	<u>0.934</u>	40.74	0.988	47.35	<u>0.993</u>
	DRSformer [14]	<u>32.17</u>	0.933	<u>41.23</u>	<u>0.989</u>	<u>48.54</u>	0.992
SSM	DFSSM	32.90	0.939	41.73	0.990	48.83	0.994

Implementation Details Our proposed DFSSM is implemented on PyTorch framework [43]. For each stage i , the number of SSGs is $N_{S_i} = 2$ and the number of FSSGs is $N_{F_i} = 2$. The initial channel C is 32. In the GDFN, the expansion rate γ is 2.0. The coefficient λ_f of the loss functions is set to 0.01.

We train our DFSSM for 300,000 iterations. The initial learning rate is fixed at $3e^{-4}$ for 92,000 iterations, then gradually decreasing to $1e^{-6}$ with the cosine annealing strategy [44]. Our model is optimized by AdamW [45] with $\beta_1 = 0.9$, $\beta_2 = 0.999$, and weight decay $= 1e^{-4}$. The batch size is 4. The patch size in training is set to 128×128 . We apply random cropping along with horizontal and vertical flipping for data augmentation.

Evaluation metrics Model performance is evaluated using peak signal-to-noise ratio (PSNR) [46] and structural similarity (SSIM) [47]. Following previous studies [8,13,14], PSNR and SSIM are measured based on the luminance channel Y of the YCbCr color space.

5.2 Comparison with state-of-the-art methods

Compared Methods We compare our DFSSM with prior-based methods (DSC [31] and GMM [32]), CNN-based methods (DDN [1], RESCAN [2], PreNet [3], MSPFN [4], RCDNet [7], MPRNet [6], CCN [8], DualGCN [9], and SPDNet [10]), and Transformer-based methods (Restormer [12], IDT [13], DRSformer [14]).

Quantitative Comparison Tab. 1 reports the quantitative results in terms of PSNR and SSIM for rain degradation removal. Our DFSSM achieves the best

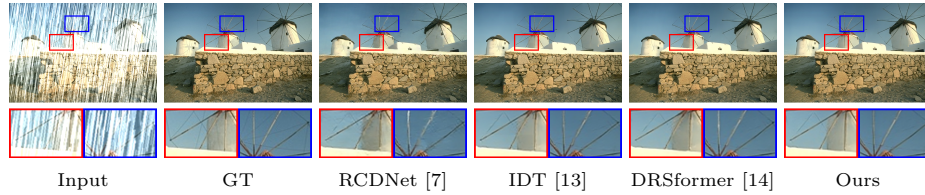


Fig. 3. Visualization comparison on the synthetic rainy image of Rain200H [28]. Red and blue boxes correspond to the zoomed-in patches.

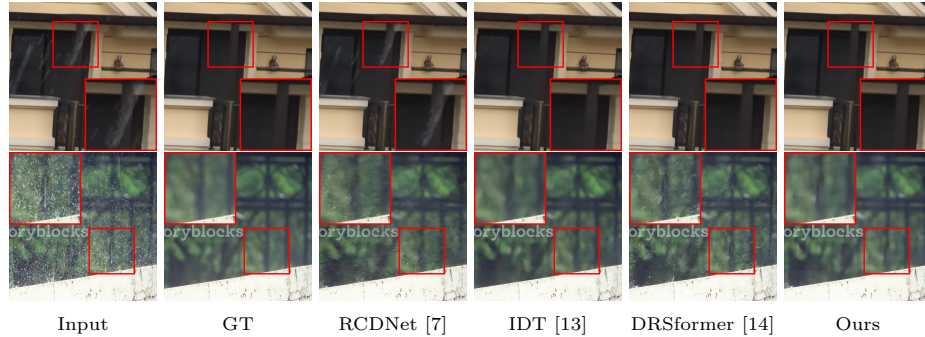


Fig. 4. Visualization comparison on the real-world rainy images of SPA-Data [29]. Red boxes correspond to the zoomed-in patches.

results across all evaluation metrics for both synthetic heavy and light rain, as well as real-world rain scenarios. In particular, our DFSSM outperforms the state-of-the-art model DRSformer [14] by 0.73dB on the Rain200H [28], 0.50dB on the Rain200L [28], and 0.29dB on the SPA-Data [29] in PSNR.

Visualization Comparison Fig. 3 visualizes the restoration results of the synthetic heavy rainy image. RCDNet [7], a CNN-based method, fails to restore the background under rainy conditions, resulting in unnatural textures, especially around windmills. Compared with Transformer-based methods, such as IDT [13] and DRSformer [14], our proposed DFSSM generates a clearer image, especially in the areas within the red boxes. As shown in Fig. 4, the results on real-world images indicate that our DFSSM achieves superior restoration outputs. In the top row images, RCDNet [7] is not able to remove some rain streaks. Observing the bottom row images, RCDNet [7] and DRSformer [14] fail to remove rain artifacts.

Model Efficiency Comparison Tab. 3 depicts the model efficiency comparison with conventional high-performing Transformer-based methods [12,13,14]. We calculate inference time for a 256×256 resolution image using a single NVIDIA GeForce RTX 2080 Ti. Compared to other methods, our DFSSM has relatively fewer parameters, but its inference time is the slowest. SSM is an

Table 2. Model efficiency comparisons.

Method	Restormer [12]	IDT [13]	DRSformer [14]	DFSSM
Parameters (M)↓	26.1	16.4	33.7	18.4
Inference Time (s)↓	0.115	0.0918	0.243	0.301

Table 3. Ablation study of the overall architecture.

Setting	FreqLoss	FSSB	MGCB	PSNR↑	SSIM↑
(a)				32.00	0.927
(b)	✓			32.36	0.932
(c)	✓	✓		32.78	0.938
(d)	✓		✓	32.82	0.938
(e)	✓	✓	✓	32.92	0.939

architecture recently adopted in deep learning, and with more optimal implementations, it holds the potential to reduce inference time significantly.

5.3 Ablation studies

In ablation studies, we train all models in the Rain200H [28] dataset under similar conditions and compare their test results using PSNR and SSIM as evaluation metrics.

Ablation study of the overall architecture To evaluate the components of the proposed DFSSM, we conducted an ablation study across five settings. This result is presented in Tab. 3. We start with the baseline [22] in setting (a). The baseline uses only the L1-Loss in its loss function, while setting (b) also uses Frequency Reconstruction Loss (FreqLoss) [26,27], resulting in improved accuracy. In setting (c), integrating FSSB into setting (b) to incorporate frequency domain processing enhances the efficacy of rain removal. Additionally, setting (d) alters the convolutional block in the baseline to the MGCB, enabling it to effectively address multi-scale rain artifacts and manage the flow of information, thereby improving performance. Setting (e), including all these improvements, surpasses the baseline with a gain of 0.92 dB in PSNR and 0.012 in SSIM.

Ablation study of FFTM Tab. 4 presents the results of an ablation study concerning the configuration of the Fast Fourier Transform Module (FFTM). Initially, to verify the effectiveness of adopting FFT, we compare it against a module without FFT. The results indicate that removing FFT degrades performance, confirming that transforming and processing in the frequency domain via FFT is effective for rain removal. Likewise, removing the spatial domain processing by 1×1 convolution with SiLU activation function before the FFT and 1×1 convolution after the IFFT deteriorates performance. Thus, these spatial domain processes are necessary.

Table 4. Ablation study of our Fast Fourier Transform Module (FFTM).

Architecture	PSNR \uparrow	SSIM \uparrow
FFTM (Tab. 3(c))	32.78	0.938
- FFT	32.57	0.935
- 1×1 conv in spatial domain	32.35	0.935

Table 5. Comparison of our Mixed-Scale Gated-Convolutional Block (MGCB) with previous convolutional blocks. CA denotes the channel attention [42].

Method	CA	PSNR \uparrow	SSIM \uparrow	Param. (M) \downarrow
GDFN [12]		32.56	0.935	17.2
MSFN [14]		32.67	0.936	20.5
GDFN [12] + CA	✓	32.71	0.938	17.3
MSFN [14] + CA	✓	32.61	0.936	20.5
MambaIR’s [22]	✓	32.36	0.932	17.1
MGCB (Tab. 3(d))	✓	32.82	0.938	17.4

Effectiveness of MGCB We compare the Mixed-Scale Gated-Convolutional Block (MGCB) with existing convolutional blocks. In the baseline [22], two 3×3 convolutions, an activation function between them, and a channel attention [42] were used. The Gated-Dconv Feed-Forward Network (GDFN) [12] comprises a gating mechanism and two 3×3 depth-wise convolutions. The Mixed-scale feed-forward network (MSFN) [14] incorporates two sets of 3×3 and 5×5 depth-wise convolutions, though it does not utilize a gating mechanism. Since GDFN and MSFN do not employ channel attention, versions with channel attention are also included in the comparison. As indicated in Tab. 5, the proposed MGCB outperforms all other methods, with slightly more parameters than GDFN [12] and MambaIR [22]’s block, and 3.1M fewer than MSFN [14]. In our MGCB, the mixed-scale convolutions and the gating mechanism work effectively.

6 Conclusion

In this paper, we present a Deraining Frequency-Enhanced State Space Model (DFSSM). To effectively remove rain artifacts, we design a Frequency-Enhanced State Space Block (FSSB), which employs a State Space Block (SSB) to model long-range dependencies and a Fast Fourier Transform Module (FFTM) for frequency domain processing in parallel. Consequently, we propose a Mixed-Scale Gated-Convolutional Block (MGCB) to capture various scale rain degradations and control the flow of features. In synthetic and real-world rain scenarios, our proposed DFSSM performs favorably against state-of-the-art algorithms quantitatively and qualitatively.

References

1. Fu, X., Huang, J., Zeng, D., Huang, Y., Ding, X., Paisley, J.: Removing rain from single images via a deep detail network. In: CVPR. (2017) 3855–3863
2. Li, X., Wu, J., Lin, Z., Liu, H., Zha, H.: Recurrent squeeze-and-excitation context aggregation net for single image deraining. In: ECCV. (2018) 254–269
3. Ren, D., Zuo, W., Hu, Q., Zhu, P., Meng, D.: Progressive image deraining networks: A better and simpler baseline. In: CVPR. (2019) 3937–3946
4. Jiang, K., Wang, Z., Yi, P., Chen, C., Huang, B., Luo, Y., Ma, J., Jiang, J.: Multi-scale progressive fusion network for single image deraining. In: CVPR. (2020) 8346–8355
5. Wang, C., Xing, X., Wu, Y., Su, Z., Chen, J.: Dcsfn: Deep cross-scale fusion network for single image rain removal. In: ACM MM. (2020) 1643–1651
6. Zamir, S.W., Arora, A., Khan, S., Hayat, M., Khan, F.S., Yang, M.H., Shao, L.: Multi-stage progressive image restoration. In: CVPR. (2021) 14821–14831
7. Wang, H., Xie, Q., Zhao, Q., Meng, D.: A model-driven deep neural network for single image rain removal. In: CVPR. (2020) 3103–3112
8. Quan, R., Yu, X., Liang, Y., Yang, Y.: Removing raindrops and rain streaks in one go. In: CVPR. (2021) 9147–9156
9. Fu, X., Qi, Q., Zha, Z.J., Zhu, Y., Ding, X.: Rain streak removal via dual graph convolutional network. In: AAAI. (2021) 1352–1360
10. Yi, Q., Li, J., Dai, Q., Fang, F., Zhang, G., Zeng, T.: Structure-preserving deraining with residue channel prior guidance. In: ICCV. (2021) 4238–4247
11. Vaswani, A., Shazeer, N., Parmar, N., Uszkoreit, J., Jones, L., Gomez, A.N., Kaiser, L., Polosukhin, I.: Attention is all you need. *NeurIPS* **30** (2017)
12. Zamir, S.W., Arora, A., Khan, S., Hayat, M., Khan, F.S., Yang, M.H.: Restormer: Efficient transformer for high-resolution image restoration. In: CVPR. (2022) 5728–5739
13. Xiao, J., Fu, X., Liu, A., Wu, F., Zha, Z.J.: Image de-raining transformer. *IEEE TPAMI* **45** (2023) 12978–12995
14. Chen, X., Li, H., Li, M., Pan, J.: Learning a sparse transformer network for effective image deraining. In: CVPR. (2023) 5896–5905
15. Chen, S., Ye, T., Bai, J., Chen, E., Shi, J., Zhu, L.: Sparse sampling transformer with uncertainty-driven ranking for unified removal of raindrops and rain streaks. In: ICCV. (2023) 13106–13117
16. Gu, A., Goel, K., Re, C.: Efficiently modeling long sequences with structured state spaces. In: ICLR. (2022)
17. Gu, A., Dao, T.: Mamba: Linear-time sequence modeling with selective state spaces. *arXiv preprint arXiv:2312.00752* (2023)
18. Zhu, L., Liao, B., Zhang, Q., Wang, X., Liu, W., Wang, X.: Vision mamba: Efficient visual representation learning with bidirectional state space model. *arXiv preprint arXiv:2401.09417* (2024)
19. Liu, Y., Tian, Y., Zhao, Y., Yu, H., Xie, L., Wang, Y., Ye, Q., Liu, Y.: Vmamba: Visual state space model. *arXiv preprint arXiv:2401.10166* (2024)
20. Huang, T., Pei, X., You, S., Wang, F., Qian, C., Xu, C.: Localmamba: Visual state space model with windowed selective scan. *arXiv preprint arXiv:2403.09338* (2024)
21. Pei, X., Huang, T., Xu, C.: Efficientvmamba: Atrous selective scan for light weight visual mamba. *arXiv preprint arXiv:2403.09977* (2024)
22. Guo, H., Li, J., Dai, T., Ouyang, Z., Ren, X., Xia, S.T.: Mambair: A simple baseline for image restoration with state-space model. *arXiv preprint arXiv:2402.15648* (2024)

23. Shi, Y., Xia, B., Jin, X., Wang, X., Zhao, T., Xia, X., Xiao, X., Yang, W.: Vmambair: Visual state space model for image restoration. arXiv preprint arXiv:2403.11423 (2024)
24. Ma, J., Li, F., Wang, B.: U-mamba: Enhancing long-range dependency for biomedical image segmentation. arXiv preprint arXiv:2401.04722 (2024)
25. Liu, J., Yang, H., Zhou, H.Y., Xi, Y., Yu, L., Yu, Y., Liang, Y., Shi, G., Zhang, S., Zheng, H., et al.: Swin-umamba: Mamba-based unet with imagenet-based pre-training. arXiv preprint arXiv:2402.03302 (2024)
26. Tu, Z., Talebi, H., Zhang, H., Yang, F., Milanfar, P., Bovik, A., Li, Y.: Maxim: Multi-axis mlp for image processing. In: CVPR. (2022) 5769–5780
27. Mao, X., Liu, Y., Liu, F., Li, Q., Shen, W., Wang, Y.: Intriguing findings of frequency selection for image deblurring. In: AAAI. (2023) 1905–1913
28. Yang, W., Tan, R.T., Feng, J., Liu, J., Guo, Z., Yan, S.: Deep joint rain detection and removal from a single image. In: CVPR. (2017) 1357–1366
29. Wang, T., Yang, X., Xu, K., Chen, S., Zhang, Q., Lau, R.W.: Spatial attentive single-image deraining with a high quality real rain dataset. In: CVPR. (2019) 12270–12279
30. Kang, L.W., Lin, C.W., Fu, Y.H.: Automatic single-image-based rain streaks removal via image decomposition. IEEE TIP **21** (2011) 1742–1755
31. Luo, Y., Xu, Y., Ji, H.: Removing rain from a single image via discriminative sparse coding. In: ICCV. (2015) 3397–3405
32. Li, Y., Tan, R.T., Guo, X., Lu, J., Brown, M.S.: Rain streak removal using layer priors. In: CVPR. (2016) 2736–2744
33. Zhang, H., Patel, V.M.: Convolutional sparse and low-rank coding-based rain streak removal. In: WACV. (2017) 1259–1267
34. Gu, S., Meng, D., Zuo, W., Zhang, L.: Joint convolutional analysis and synthesis sparse representation for single image layer separation. In: ICCV. (2017) 1708–1716
35. Liu, H., Simonyan, K., Yang, Y.: DARTS: Differentiable architecture search. In: ICLR. (2019)
36. Ronneberger, O., Fischer, P., Brox, T.: U-net: Convolutional networks for biomedical image segmentation. In: MICCAI. (2015) 234–241
37. Shi, W., Caballero, J., Huszár, F., Totz, J., Aitken, A.P., Bishop, R., Rueckert, D., Wang, Z.: Real-time single image and video super-resolution using an efficient sub-pixel convolutional neural network. In: CVPR. (2016) 1874–1883
38. Chi, L., Jiang, B., Mu, Y.: Fast fourier convolution. NeurIPS **33** (2020) 4479–4488
39. Zhang, D., Huang, F., Liu, S., Wang, X., Jin, Z.: Swinfir: Revisiting the swinir with fast fourier convolution and improved training for image super-resolution. arXiv preprint arXiv:2208.11247 (2022)
40. Elfwing, S., Uchibe, E., Doya, K.: Sigmoid-weighted linear units for neural network function approximation in reinforcement learning. Neural networks **107** (2018) 3–11
41. Hendrycks, D., Gimpel, K.: Gaussian error linear units (gelus). arXiv preprint arXiv:1606.08415 (2016)
42. Hu, J., Shen, L., Sun, G.: Squeeze-and-excitation networks. In: CVPR. (2018) 7132–7141
43. Paszke, A., Gross, S., Massa, F., Lerer, A., Bradbury, J., Chanan, G., Killeen, T., Lin, Z., Gimelshein, N., Antiga, L., et al.: Pytorch: An imperative style, high-performance deep learning library. NeurIPS **32** (2019)
44. Loshchilov, I., Hutter, F.: SGDR: Stochastic gradient descent with warm restarts. In: ICLR. (2017)

- 45. Loshchilov, I., Hutter, F.: Decoupled weight decay regularization. In: ICLR. (2019)
- 46. Huynh-Thu, Q., Ghanbari, M.: Scope of validity of psnr in image/video quality assessment. *Electronics letters* **44** (2008) 800–801
- 47. Wang, Z., Bovik, A.C., Sheikh, H.R., Simoncelli, E.P.: Image quality assessment: from error visibility to structural similarity. *IEEE TIP* **13** (2004) 600–612